Velocity–Azimuth Display Analysis of Doppler Velocity for HIWRAP

LIN TIAN

NASA Goddard Space Flight Center, Greenbelt, and Goddard Earth Sciences Technology and Research, Morgan State University, Baltimore, Maryland

GERALD M. HEYMSFIELD

NASA Goddard Space Flight Center, Greenbelt, Maryland

ANTHONY C. DIDLAKE JR.

NASA Goddard Space Flight Center, Greenbelt, Maryland, and Oak Ridge Associated Universities, Oak Ridge, Tennessee

STEPHEN GUIMOND

NASA Goddard Space Flight Center, Greenbelt, and University of Maryland, College Park, College Park, Maryland

LIHUA LI

NASA Goddard Space Flight Center, Greenbelt, Maryland

(Manuscript received 13 March 2014, in final form 7 May 2015)

ABSTRACT

The velocity–azimuth display (VAD) analysis technique established for ground-based scanning radar is applied to the NASA High-Altitude Imaging Wind and Rain Airborne Profiler (HIWRAP). The VAD technique provides a mean vertical profile of the horizontal winds for each complete conical scan of the HIWRAP radar. One advantage of this technique is that it has shown great value for data assimilation and for operational forecasts. Another advantage is that it is computationally inexpensive, which makes it suitable for real-time retrievals. The VAD analysis has been applied to the HIWRAP data collected during NASA's Genesis and Rapid Intensification Processes (GRIP) mission. The traditional dual-Doppler analysis for deriving wind fields in the nadir plane is also presented and is compared with the VAD analysis. The results show that the along-track winds from the VAD technique and dual-Doppler analysis agree in general. The VAD horizontal winds capture the mean vortex structure of two tropical cyclones, and they are in general agreement with winds from nearby dropsondes. Several assumptions are made for the VAD technique. These assumptions include a stationary platform for each HIWRAP scan and constant vertical velocity of the hydrometeors along each complete scan. As a result, the VAD technique can produce appreciable errors in regions of deep convection such as the eyewall, whereas in stratiform regions the retrieval errors are minimal. Despite these errors, the VAD technique can still adequately capture the larger-scale structure of the hurricane vortex given a sufficient number of flight passes over the storm.

1. Introduction

Airborne Doppler radars have been used for studying winds in precipitation systems for nearly 30 years. Most of the studies used data from single- or dual-beam Doppler radars that were either scanning in a plane normal to the aircraft track or about 20° fore and aft of the plane normal to the fuselage [e.g., National Oceanic and Atmospheric Administration (NOAA) WP-3D tail radar (Jorgensen et al. 1983, 1996) and National Center for Atmospheric Research (NCAR) Electra Doppler Radar (ELDORA; Hildebrand et al. 1996)]. With this scanning geometry, the fore and aft Doppler velocity information is used to derive two components of the three-dimensional wind field.

Corresponding author address: Anthony Didlake, NASA Goddard Space Flight Center, Code 612, Greenbelt, MD 20771.
E-mail: anthony.didlake@nasa.gov

DOI: 10.1175/JAMC-D-14-0054.1

The remaining third component, which is usually the vertical velocity, is obtained by integrating the mass continuity equation with boundary conditions at the surface or cloud top, or both. The dual-Doppler synthesis for this type of scanning radar has been well studied, and many studies have been conducted using this approach on ELDORA and P3 radar data to derive structure in tropical storms that requires accurate representations of the three-dimensional winds (e.g., Jorgensen et al. 1983; Ray et al. 1985; Marks and Houze 1987; Chong and Testud 1996). The dual-Doppler synthesis procedures have also been implemented in the NCAR software package Custom Editing and Display of Reduced Information in Cartesian (CEDRIC) (Mohr et al. 1986), which is widely used by the meteorological community.

A new airborne scanning Doppler radar, the High-Altitude Imaging Wind and Rain Airborne Profiler (HIWRAP), has been developed recently at NASA Goddard Space Flight Center (Li et al. 2008). It is a downward-pointing, conically scanning Doppler radar system with dual frequency (Ku and Ka bands) and dual beams (30° and 40° incidence angles), with the capability to provide information about three-dimensional reflectivity and wind structures in precipitating systems and ocean surface winds in rain-free regions. HIWRAP was designed to fly on board NASA's Global Hawk Unmanned Aerial System, which, unlike other Doppler radar–equipped aircraft, can provide extended coverage of precipitation targets for over 24 h. The HIWRAP flew on NASA's Global Hawk Unmanned Aerial System for the first time in the summer of 2010 during the NASA Genesis and Rapid Intensification Processes (GRIP) field campaign (Braun et al. 2013).

As the scanning geometry of HIWRAP is different from the previous airborne Doppler scanning radars, it is important to examine the applicability and the limitations of established methods for HIWRAP. In a recent paper by Guimond et al. (2014), an algorithm for the retrieval of three-dimensional wind fields from downward-pointing, conically scanning airborne Doppler radars is presented. This method is a global solver based on minimizing a cost function between modeled and observed radial velocities with possible dynamic constraints (e.g., Gamache 1997; Gao et al. 1999). Didlake et al. (2015) presented an alternative retrieval method that is based on the coplane technique described by Armijo (1969) and Miller and Strauch (1974). This method is a local solver that uses mass continuity and appropriate boundary conditions to retrieve the three-dimensional wind field in a coordinate system natural to the radar scanning geometry. In this paper, we will focus on the velocity–azimuth display (VAD) method applied to the HIWRAP scanning geometry. We will also discuss and compare the application of the traditional dual-Doppler analysis for deriving wind fields in the nadir plane and estimating horizontal wind divergence.

The VAD technique, first developed by Lhermitte and Atlas (1961) and Browning and Wexler (1968), has been used to obtain the mean vertical profile of the horizontal winds from ground-based Doppler radars in situations of widespread precipitation. Under the assumption that the horizontal wind field at a given altitude is linear within the regions scanned by the radar, the radial wind data are fitted to a sinusoidal curve as a function of azimuth for fixed elevations. Improvements of the VAD technique include the extended VAD (e.g., Srivastava et al. 1986; Matejka and Srivastava 1991) for extracting additional parameters such as divergence and vertical wind fields.

There are several operational and research applications that motivate the use of the VAD technique on HIWRAP observations. One of the important applications is using VAD-derived horizontal wind fields for data assimilation (e.g., Michelson and Seaman 2000; Gao et al. 2004; Sun and Zhang 2008). As a proof-of-concept study, Sippel et al. (2013) showed that simulated HIWRAP Doppler velocity observations could potentially improve hurricane analysis and prediction. However, when data from real hurricane observations were used, it was found that VAD-derived wind fields produced more promising results in terms of predicting the track, maximum intensity, and size of the hurricane in comparison with using Doppler velocity directly (Sippel et al. 2014). Another application of the VAD-derived wind fields is to provide the vertical wind structure of precipitation regions for general context purposes. The VAD technique provides the mean horizontal wind at high vertical resolution, which can be used in case studies to establish the overall structure of the analyzed convection. Last, the VAD technique is a computationally quick method such that it is suitable for real-time retrievals of the mean wind field. These retrievals can be used for making real-time flight decisions and providing forecasters with information on the storm's center location and overall wind structure in near–real time.

HIWRAP has a scanning geometry that is suitable for the VAD analysis; however, several aspects of HIWRAP make the VAD analysis different from that for ground-based radars: 1) on a moving platform, a complete rotation of the radar beam traces a section of a spiral, and 2) HIWRAP scans at fixed high elevation angles. These can cause errors in VAD-derived horizontal wind fields. The objective of this paper is to understand and address those issues and to develop procedures of a VAD analysis directly related to HIWRAP scanning geometry. The long-term goal is to implement a real-time VAD algorithm on the Global Hawk to obtain tropical cyclone mean wind

TABLE 1. HIWRAP system specifications during GRIP.

Parameters	Specifications	
	Ku band	Ka band
Radio frequency (GHz)	Inner beam: 13.910 Outer beam: 13.470	Inner beam: 35.560 Outer beam: 33.720
Transmitter peak power (W)	25	8
Beamwidth (°)	2.9	1.2
Beam pointing angle (° off nadir)	30 (inner), 40 (outer)	Same as Ku
Polarization	H (inner beam), V (outer beam)	Same as Ku
PRF (Hz)	4000, 5000	Same as Ku
Transmitter pulse width (μs)	0–40	Same as Ku
Range bin (m)	150	Same as Ku
Detection range (km)	20	Same as Ku
Min detected reflectivity (dBZ_e; 60-m range resolution, 10-km range, and 3-km chirp pulse)	0.0	−5.0
Dynamic range (dB)	>65	Same as Ku
Doppler velocity (m s^{-1})	0–96 (accuracy < 1.5 m s^{-1} for SNR > 10)	Same as Ku
Scanning	Conical scan, 16 rpm	Same as Ku

structures that are suitable for data assimilation and improving forecasts of intensity change and track.

Section 2 briefly describes the HIWRAP radar system, its scanning geometry, and equations for mapping observations from aircraft-relative to flight-track-relative coordinates. Section 3 presents the VAD retrieval method and the dual-Doppler method for HIWRAP. The application of the VAD analysis to HIWRAP observations of Tropical Storm Matthew and Hurricane Karl is presented in section 4. An error analysis and discussion of tropical cyclone research applications is given in section 5, followed by the conclusions in section 6.

2. The HIWRAP radar, scanning geometry, and coordinate mapping

a. The radar and scanning geometry

The HIWRAP radar was designed to fly on board high-altitude, long-endurance platforms such as the Global Hawk where wind and precipitation measurements can be obtained with high spatial resolution over an extended time period. The HIWRAP system flew on Global Hawk AV-6 during GRIP, and its specifications are given in Table 1. It is a dual-beam and dual-frequency scanning Doppler radar system. The two beams point at fixed incidence angles of 30° and 40° from nadir. Each beam operates at both Ku-band (14 GHz) and Ka-band (35 GHz) frequencies. The scans of HIWRAP are similar to conical scans from a ground-based radar but looking downward. The azimuth rotation rate of the antenna is approximately 90° s^{-1}, so that one complete revolution takes about 4 s. Combining the antenna rotation rate with the Global Hawk's nominal ground speed (~176 m s^{-1}), the aircraft moves approximately 700 m when completing one scan circle. The typical along-beam range resolution during the GRIP was 150 m.

Assuming a nominal aircraft altitude of 19 km, and for the moment ignoring the translation of the aircraft, the intersection of the radar beams with the surface would be concentric circles of radii about 11 km (30° beam) and 16 km (40° beam). If the aircraft flies along an *ideal* straight horizontal line, the radar beams would sweep out spiral paths as shown in Fig. 1a. From the beam trajectories it is clear that many observations are obtained at coincident or near-coincident points. In practice, perturbations to the ideal flight track, such as nonzero pitch, roll, and drift angles, are common because of environmental conditions (i.e., turbulence). Therefore, the actual beam trajectory has small deviations from the trajectories shown in Fig. 1a. This necessitates various corrections, which are outlined below.

b. Coordinate mapping

To remove the aircraft motion from the Doppler velocities, and also for subsequent wind retrievals, we need to map the HIWRAP data from aircraft- to track-relative coordinates. We follow the approach of Lee et al. (1994) and define two coordinate systems: aircraft-relative $[X_a = (x_a, y_a, z_a)]$ and track-relative $[X_t = (x_t, y_t, z_t)]$ coordinates. The X_a system is defined as follows: $+x_a$ is along the right wing, $+y_a$ is along the fuselage through the nose, and $+z_a$ is up along the tail stabilizer. In the X_t coordinate system, $+y_t$ points along the flight track (the motion vector of the aircraft projected on the horizontal plane), $+x_t$ points 90° to the right of the $+y_t$, and $+z_t$ points to the local zenith. The origins of the

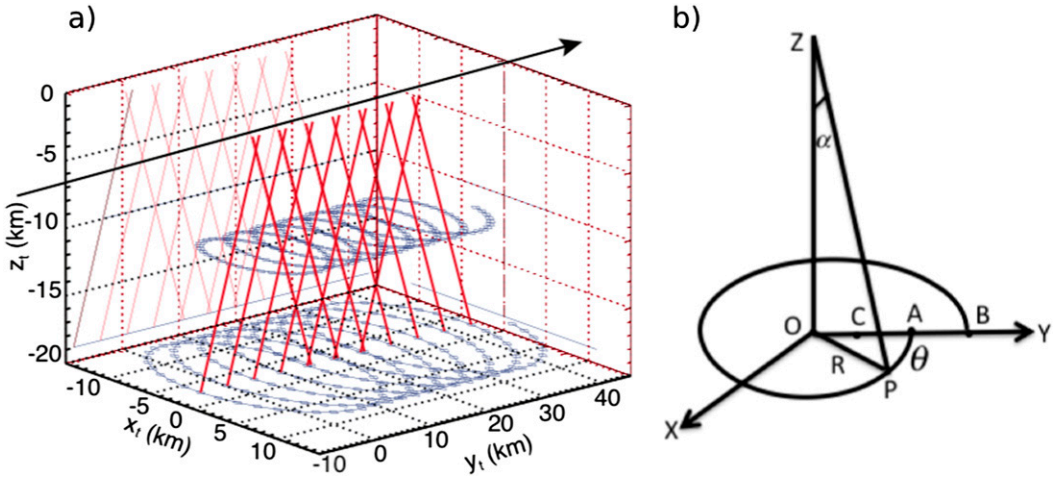

FIG. 1. (a) Beam trajectory (blue) at two different heights for HIWRAP at incidence angle of 30°. The red line shows the fore and aft beams in the vertical cross section under the flight track. (b) HIWRAP scanning geometry: the letter O is directly below the aircraft; $x = x_0$, $y = y_0$, and $t = t_0$ at O. The letter A is the radar beam position at $t = t_0$ and $\theta = 0$. The is the radar beam position at $t = t_0 + \tau$, where $\tau = 2\pi/\Omega$ is the time for one complete revolution. The C is the position of radar directly below the aircraft at $t = t_0 + \tau$. The P is the beam position at $\theta(t) = \Omega t$, and $\Omega = 1.67\ \mathrm{s}^{-1}$ is the antenna azimuth rotation rate.

coordinate systems can be some arbitrary point along the flight track. Other details can be found in Lee et al.'s (1994) paper. All the radar scans are bound to the aircraft frame. Therefore, the location of each radar data point is given in the aircraft-relative coordinates in terms of a rotation angle θ_a measured clockwise from $+y_a$ in the horizontal projection of the radar beam, an elevation angle $\Phi_a = -(\pi/2 - \tau_a)$, and range r. The term τ_a (=30° and 40° for HIWRAP) is the angle between the radar beam and negative z_a. Note that the convention for elevation angle is the same as that for ground-based radars; that is, a negative elevation angle means that the antenna points downward from the horizontal. For the HIWRAP scanning geometry,

$$X_a = \begin{pmatrix} x_a \\ y_a \\ z_a \end{pmatrix} = r \begin{pmatrix} \cos\Phi_a \sin\theta_a \\ \cos\Phi_a \cos\theta_a \\ \sin\Phi_a \end{pmatrix}. \qquad (1)$$

Equation (1) is different from the corresponding Eq. (4) in Lee et al. (1994) since HIWRAP scans around the vertical z_a axis rather than the horizontal y_a axis, which was the case with the NOAA P3 tail radar and the NCAR ELDORA airborne radars discussed by Lee et al. (1994). The transformation between X_a and X_t is derived using Eq. (8) in Lee et al.'s (1994) paper. The elevation angle Φ_t and rotation angle θ_t in track-relative coordinates are given by $\sin\Phi_t = z_t/r$ and $\cos\theta_t = (y_t - U_a t)/\sqrt{x_t^2 + (y_t - U_a t)^2}$, where U_a is the aircraft speed and t the time elapsed from the start of the flight line.

3. Wind retrieval methods for HIWRAP

We now discuss methods for retrieving wind fields from HIWRAP Doppler velocity data. First, we note that the fore and aft directions of a given scan have many intersections in the vertical plane below the flight path (Fig. 1a). The Doppler velocities observed at these points can be used to calculate the components of the particle velocity in the vertical plane. The same result can be obtained by using two fixed beams, pointing at nadir and forward, as is done in the ER-2 airborne Doppler radar system (Heymsfield et al. 1996).

To realize the full potential of the HIWRAP system, we need to make use of the three-dimensional Doppler velocity data. Below, we discuss two methods for processing these data. The methods are based on VAD and dual-Doppler radar analysis techniques used for ground-based radars. Note that all the subsequent discussion will be in track-relative coordinates, so we will drop subscript t from all the track-relative symbols.

a. VAD analysis

For stationary ground-based radars, the horizontal section of a complete conical scan is a circle. For HIWRAP, the scans are affected by aircraft motion, which can be resolved into a constant translational motion and superimposed fluctuating motions due to changes in altitude, roll and pitch angles, and the ground speed of the plane. Because of the translational motion, a complete rotation of the radar beam traces a section of a spiral on a horizontal plane.

Figure 1b shows a schematic of a VAD circle with center at (x_0, y_0, z_0). Positions along the circle can be specified by the rotation angle θ and elevation angle $\Phi = -(\pi/2 - \alpha)$. The radial velocity V_r along the VAD circle is given by

$$V_r(\theta) = u\cos\Phi\sin\theta + v\cos\Phi\cos\theta - W\sin\Phi. \quad (2)$$

Note that both θ and Φ are in track-relative coordinates. Since the variation of Φ is small ($<2°$) because of the high stability of the aircraft, we assume it is constant. The velocity components in the x, y, z directions are denoted by u, v, W, where $W = w + V_T$, w is the vertical wind, and V_T is the terminal velocity. Note that W, w, and V_T are defined as positive downward. Similar to Browning and Wexler (1968), we assume that the horizontal wind field is linear and the vertical wind field is a constant over each scan circle:

$$\begin{aligned} u &= u_0 + u_x(x - x_0) + u_y(y - y_0), \\ v &= v_0 + v_x(x - x_0) + v_y(y - y_0), \quad \text{and} \\ W &= W_0. \end{aligned} \quad (3)$$

Here, (u_0, v_0, W_0) is the particle velocity, and the subscripts x and y denote derivatives at the center of the circle. Note that the linear expansion of u and v is around the center of the VAD circle. Therefore, for each VAD circle along the flight line, the linear expansion is not around a stationary point. At any point $P(x, y)$ along the scan circle for HIWRAP whose scan center moves along track with time (see Fig. 1b),

$$\begin{aligned} x - x_0 &= r\cos\Phi\sin\theta \quad \text{and} \\ y - y_0 &= r\cos\Phi\cos\theta + \left(\frac{U_a\tau}{2\pi}\right)\theta, \end{aligned} \quad (4)$$

where U_a is the aircraft ground speed and τ is the time period for the antenna to complete one rotation. From Eqs. (2)–(4), we have

$$\begin{aligned} V_r(\theta) = {} & C_0 + C_1\cos\theta + C_2\sin\theta + D_1\cos(2\theta) \\ & + D_2\sin(2\theta) + E_1(\theta\cos\theta) + E_2(\theta\sin\theta), \end{aligned} \quad (5)$$

with

$$\begin{aligned} & C_0 = W_0\sin\Phi + \mathrm{DIV}_h\frac{R\cos\Phi}{2}, \quad C_1 = v_0\cos\Phi, \quad C_2 = u_0\cos\Phi, \\ & D_1 = \frac{R\cos\Phi}{2}(v_y - u_x), \quad D_2 = \frac{R\cos\Phi}{2}(u_y + v_x), \\ & E_1 = \cos\Phi\frac{U_a\tau}{2\pi}v_y, \quad \text{and} \quad E_2 = \cos\Phi\frac{U_a\tau}{2\pi}u_y, \end{aligned} \quad (6)$$

where $R = r\cos\Phi$, and $\mathrm{DIV}_h = u_x + v_y$ is the divergence of the horizontal wind; D_1 and D_2 are related to the deformation of the horizontal wind. The displacement of the scan "center" during one complete revolution of the beam, $U_a\tau$, is about 650 m. This displacement is small compared to the diameter of the scan "circle," which is about 22 km (34 km) at the ground for incidence angle 30° (40°). Thus, we may approximate the open curve by a closed circle by assuming $U_a\tau \sim 0$. Under this assumption, Eq. (5) is the same as the standard VAD methods used for ground-based radars (e.g., Browning and Wexler 1968).

For ground-based radars scanning at low elevation angles, the $W_0\sin\Phi$ term in the expression for C_0 in Eq. (6) is neglected, thus giving the DIV_h directly. The vertical air velocity is then obtained by integrating the continuity equation using zero vertical air velocity at or near the ground as the boundary condition. For HIWRAP, the elevation angle is not small; therefore the $W_0\sin\Phi$ term cannot be neglected. In this case, we can use the vertical particle velocity estimated from observations by the scanning beam when it is pointed in the fore and aft directions of the flight path that will be discussed in section 3b.

We now consider the error due to the VAD circle not being a perfect circle because of aircraft motion. For $U_a = 0$ and $E_1 = E_2 = 0$, we have the standard VAD. Fourier analysis gives coefficients C_0, C_1, C_2, D_1, and D_2:

$$\begin{aligned} & C_0 = \frac{1}{2\pi}\int_0^{2\pi} V_r(\theta)\,d\theta, \quad C_1 = \frac{1}{\pi}\int_0^{2\pi} V_r(\theta)\cos\theta\,d\theta, \\ & C_2 = \frac{1}{\pi}\int_0^{2\pi} V_r(\theta)\sin\theta\,d\theta, \quad D_1 = \frac{1}{\pi}\int_0^{2\pi} V_r(\theta)\cos2\theta\,d\theta, \\ & \text{and} \quad D_2 = \frac{1}{\pi}\int_0^{2\pi} V_r(\theta)\sin2\theta\,d\theta. \end{aligned} \quad (7)$$

From those coefficients, we can get u_0, v_0, $v_y - u_x$, $u_y + v_x$, and DIV_h if W_0 is known. For $U_a \neq 0$ (and thus $E_1 \neq 0$, $E_2 \neq 0$), we can assume $V_r(\theta)$ as though we have a perfect VAD circle to calculate coefficients C_0^*, C_1^*, C_2^*, D_1^*, D_2^* using Eq. (7) and then estimate u_0^*, v_0^*, DIV_h^*, $v_y^* - u_x^*$, and $u_y^* + v_x^*$ from Eq. (6). We can then estimate the errors in these coefficients

from the ''true'' values. Using Eqs. (5), (6), and (7), we have

$$\mathrm{DIV}_h^* = \mathrm{DIV}_h - \frac{U_a\tau}{\pi R}u_y, \tag{8}$$

$$v_0^* = \frac{1}{\cos\Phi}\left(C_1 + E_1\pi - \frac{E_2}{2}\right) = v_0 + \frac{U_a\tau}{2}\left(v_y - \frac{1}{2\pi}u_y\right), \tag{9}$$

$$u_0^* = \frac{1}{\cos\Phi}\left(C_2 - \frac{E_1}{2} + \pi E_2\right) = u_0 + \frac{U_a\tau}{2}\left(\frac{1}{2\pi}v_y - u_y\right), \tag{10}$$

$$v_y^* - u_x^* = v_y - u_x + \frac{2U_a\tau}{3\pi R}u_y, \quad \text{and} \tag{11}$$

$$u_y^* + v_x^* = u_y + v_x - \frac{4U_a\tau}{3\pi R}v_y. \tag{12}$$

From Eqs. (8)–(12), we can estimate the errors due to the VAD circle not being a perfect circle because of aircraft motion. We defined these errors as $\delta(u_0) = |u_0^* - u_0|$ for u_0, and $\delta(\mathrm{DIV}_h) = |\mathrm{DIV}_h^* - \mathrm{DIV}_h|$ and similar definitions for other parameters. Those errors depend on aircraft ground speed, antenna rotation rate, and horizontal wind gradient. Errors in divergence and deformation also depend on the range from the radar. For HIWRAP observations, $\tau = 2\pi/\Omega = 3.75$ s, $U_a = 176\,\mathrm{m\,s^{-1}}$, and $U_a\tau = 660$ m. Divergence observed in tropical cyclone rainbands is about $10^{-4}\,\mathrm{s^{-1}}$ for stratiform rain and $10^{-3}\,\mathrm{s^{-1}}$ for convective rain (e.g., Didlake and Houze 2009, 2013). Based on those numbers, we assume a horizontal wind gradient of $1\,\mathrm{m\,s^{-1}}$ over 1 km horizontal distance (i.e., $v_y = u_y \sim 10^{-3}\,\mathrm{s^{-1}}$). These numbers give $|\delta(u_0)| = |\delta(v_0)| \sim 0.38\,\mathrm{m\,s^{-1}}$. Figure 2 shows that the errors in horizontal divergence and deformation vary between 10^{-5} and $10^{-4}\,\mathrm{s^{-1}}$ for a range between 3 and 18 km, which is between 1% and 10% of a typical value of $10^{-3}\,\mathrm{s^{-1}}$ for those parameters. For example, at $r = 16$ km, we have $|\delta(\mathrm{DIV}_h)| \sim 1.5\times10^{-5}\,\mathrm{s^{-1}}$, and $|\delta(v_y - u_x)| \sim 1\times10^{-5}\,\mathrm{s^{-1}}$. We can see that in the tropical cyclone rainband regions, errors in u_0 and v_0 due to the ''closed'' circle approximation are less than $0.5\,\mathrm{m\,s^{-1}}$, and errors in derivative terms are less than 10% of the derivative term magnitudes.

In the tropical cyclone eyewall region, divergence values, and thus wind errors due to the closed circle approximation, can be an order of magnitude higher than in the rainband regions. While these errors still remain a small fraction of eyewall wind speeds, additional errors can occur in the eyewall region, which calls for judicious use of the VAD technique here. We have found that horizontal wind errors from the assumption that W is constant across the scan circle can reach $10\,\mathrm{m\,s^{-1}}$. This error is discussed in detail in section 5.

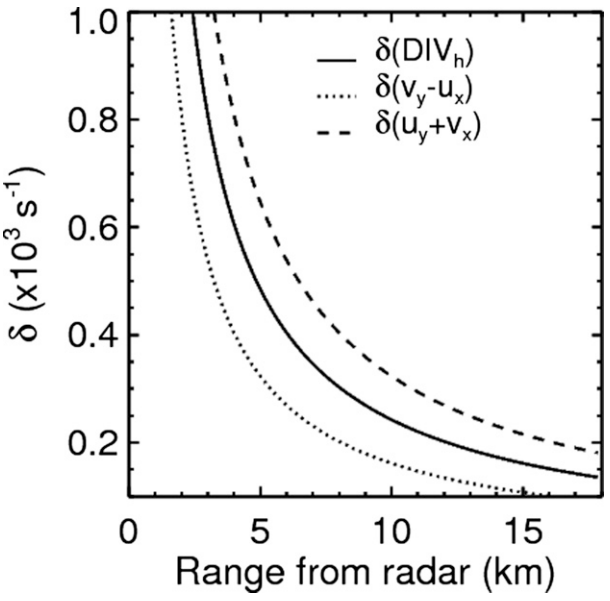

FIG. 2. Errors in DIV_h and deformations due to aircraft motion for a horizontal wind gradient of $10^{-3}\,\mathrm{s^{-1}}$. The errors are plotted as a function of range from the radar. See the text for details.

b. *Dual-Doppler analysis*

In this section, we discuss a dual-Doppler analysis method that provides two components of the particle velocity. This method incorporates the Doppler velocities measured from the fore and aft looks of HIWRAP along the aircraft track, which may be regarded as independent observations. For this study, the retrieved two components are calculated only in the nadir plane beneath the aircraft; moreover, they are used for comparisons with the VAD retrieval and for estimating the VAD-derived horizontal wind divergence.

The dual-Doppler method, well established for ground-based radars, uses a cylindrical coordinate system with the radar baseline as the axis of the coordinate system (e.g., Armijo 1969; Miller and Strauch 1974). For the HIWRAP scanning geometry, we can set up a cylindrical coordinate system as shown in Fig. 3. Chong and Testud (1996) used a similar approach for ELDORA. The flight track is chosen as the axis of the coordinate system and an arbitrary point O as its origin. Any point P is specified by its radial (ρ), azimuthal (α), and axial (Y) coordinates. Note that the Y axis is along the flight track. The azimuthal coordinate, or the coplane angle, is measured clockwise from the nadir plane. The track-relative Cartesian coordinate system (x, y, z) with the same origin has its y axis coincident with the Y axis, the z axis vertically up, and the x axis to the right of y in the horizontal plane. The particle velocity components in the cylindrical and Cartesian systems are denoted by (U_ρ, U_α, U_Y) and (u, v, W), respectively. The velocity components are related as follows:

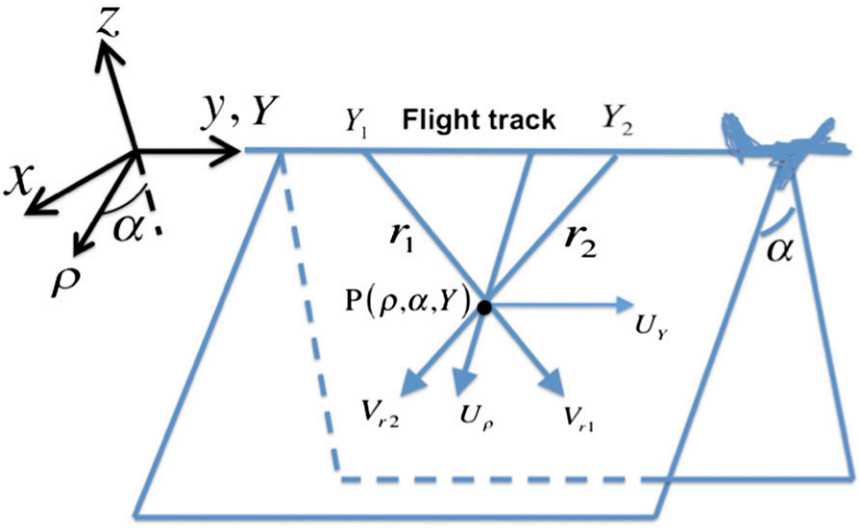

FIG. 3. Cylindrical coordinate system used for HIWRAP for dual-Doppler radar analysis. The P is position of the target. The quantities r_1 and r_2 are the ranges from radar at positions Y_1 and Y_2 along the flight track to P. The quantities Y, ρ, and α are respectively the cylindrical axis along the flight track, range from the axis to grid point P, and coplane angle. The quantities U_ρ and U_Y are the wind components on the coplane. The quantities V_{r_1} and V_{r_2} are the mean radial Doppler velocities at gridpoint P. The corresponding Cartesian coordinate system (x, y, z) has the y axis coincident with the Y axis, the z axis is vertically up, and the x axis is to the right of y in the horizontal plane.

$$U_Y = v, \quad U_\rho = u\sin\alpha - W\cos\alpha, \quad U_\alpha = u\cos\alpha + W\sin\alpha,$$
$$u = U_\rho\sin\alpha + U_\alpha\cos\alpha, \quad v = U_Y, \quad \text{and}$$
$$W = U_\alpha\sin\alpha - U_\rho\cos\alpha. \tag{13}$$

Suppose that the Doppler velocity at the point P is measured to be V_{r_1} when the radar is at $(0, 0, Y_1)$ and V_{r_2} when the radar is at $(0, 0, Y_2)$. These two measurements are separated in time by $(Y_2 - Y_1)/U_\alpha$, where U_a is the speed of the aircraft. The radial velocities are given by

$$V_{r_1} = [\rho U_\rho + (Y - Y_1)U_Y]/r_1 \quad \text{and}$$
$$V_{r_2} = [\rho U_\rho + (Y - Y_2)U_Y]/r_2, \tag{14}$$

where $r_1 = \sqrt{\rho^2 + (Y - Y_1)^2}$, $r_2 = \sqrt{\rho^2 + (Y - Y_2)^2}$, and Y is the position of point P along the Y axis. The equations in Eq. (14) can be solved for the components of the particle velocity in the coplane:

$$U_\rho = \frac{-r_1(Y - Y_2)V_{r_1} + r_2(Y - Y_1)V_{r_2}}{\rho(Y_2 - Y_1)} \quad \text{and}$$
$$U_Y = \frac{r_1 V_{r_1} - r_2 V_{r_2}}{(Y_2 - Y_1)}. \tag{15}$$

To determine U_α, we need to integrate the continuity equation using a boundary condition. In the case of ground-based radars, the boundary condition $w = 0\,\mathrm{m\,s^{-1}}$ at the ground can be applied easily since the ground happens to be a coplane. In our case, the corresponding coplane is the nadir plane, and the corresponding boundary condition would be the winds perpendicular to the nadir plane. While these winds are not readily known, Didlake et al. (2015) discuss a method for retrieving these winds in the nadir plane and the U_α component throughout the domain.

Various errors may degrade the synthesized wind field calculated from dual-Doppler analysis. Procedures to determine these errors are described in Testud et al. (1995). For HIWRAP, we consider a special case in which the two beams intersect at the same elevation angle:

$$W = -(V_{r_1} + V_{r_2})/2\sin\Phi \quad \text{and}$$
$$v = (V_{r_1} - V_{r_2})/2\cos\Phi. \tag{16}$$

Note that Φ is the elevation angle in track coordinates, which can differ from the aircraft-relative elevation angle by a few degrees. Observations from GRIP show that variation in Φ is about $\pm 2°$ because of changes of the aircraft roll and pitch angles. Assuming $\Phi = -60°$, such variation in Φ will result in a 2% error in W and 3% error in v. In general, the standard error due to signal fluctuations is small. Using the HIWRAP radar parameters in Table 1, we estimated standard errors in mean Doppler velocity V_r due to signal fluctuations to

be $\sigma(V_r) = 1.46\ (0.46)\ \mathrm{m\,s^{-1}}$ for Ku (Ka) band. From Eq. (16), we have

$$\sigma^2(v) = \frac{\sigma^2(V_r)}{2\sin^2\Phi} \quad \text{and} \quad \sigma^2(W) = \frac{\sigma^2(V_r)}{2\cos^2\Phi}. \tag{17}$$

Substituting those numbers into Eq. (17), we have, for $\Phi = -60°$, $\sigma(v) = 1.2\ (0.4)\ \mathrm{m\,s^{-1}}$ for Ku (Ka) band, and $\sigma(W) = 2\ (0.6)\ \mathrm{m\,s^{-1}}$ for Ku (Ka) band. For $\Phi = -50°$, $\sigma(v) = 1.3\ (0.4)\ \mathrm{m\,s^{-1}}$ for Ku (Ka) band, and $\sigma(W) = 1.6\ (0.5)\ \mathrm{m\,s^{-1}}$ for Ku (Ka) band.

4. Application of VAD analysis to GRIP data

a. Data description

The GRIP field experiment was the first time that HIWRAP collected data in tropical cyclones, amassing detailed observations from 20 transects across the eye of Hurricane Karl and 11 transects across Tropical Storm Matthew. As this was HIWRAP's first science mission, there were a few unexpected data quality issues that we had to account for in our analysis. First, only inner-beam (30° incidence) data are available from the GRIP flights. The inner beam has a smaller scan circle (22 km in diameter at the surface) than the outer beam (32 km in diameter at the surface). The inner-beam data may be more suitable for the VAD analysis as the assumptions of linear wind fields and constant vertical velocity are better approximations for the smaller scan circle. Another issue is that the Ka-band data contained excessive noise due to a digital receiver firmware issue, which made it difficult to properly unfold the Doppler data. As a result, the current analysis focuses solely on the Ku-band observations. Last, pulse compression range sidelobes contaminated the Doppler velocity data collected below ~2-km altitude. This study will focus on data analyses above 2-km altitude. We must emphasize that these data quality issues are particular to the current GRIP dataset. In the time since GRIP, HIWRAP missions have acquired data with significantly improved quality due to a number of upgrades and fixes, such as the digital receiver firmware, improved-range sidelobes, and blending of the pulse and chirp returns to provide better observations near the surface and above 15 km.

Procedures for processing GRIP data from the Global Hawk are very similar to those for the HIWRAP data collected from the ER-2 (Heymsfield et al. 2013). However, one significant difference is that the antenna on the Global Hawk rotates, while on the ER-2 the antennas are fixed. As a result of the scanning antenna, only 64 samples are used to estimate Doppler velocity using the pulse-pair technique, which leads to lower sensitivity and noisier Doppler velocities. Also, the aircraft ground speed has a much larger contribution to the Doppler radial velocity from the scanning HIWRAP because of its high elevation angle, and the Doppler velocity is usually folded because of the limited Nyquist velocity interval. The aircraft motion is first removed from the raw Doppler velocity following the procedure outlined by Lee et al. (1994). Modifications to Lee et al. (1994) for the HIWRAP scanning geometry and angle definitions are derived and presented in Eqs. (5) and (6) of Guimond et al. (2014). The Doppler velocity is then unfolded using a dual-PRF algorithm described in detail in Dazhang et al. (1984). Other corrections have been made to the Doppler velocities: 1) antenna-pointing biases have been corrected by comparing the measured Doppler velocity at the surface and radial components due to the aircraft motion, 2) data with aircraft roll angles $> 3°$ have been eliminated to ensure the selected flight line is straight and level, and 3) velocities are discarded when the echo power is lower than a specified threshold value necessary to obtain a reliable velocity estimate. We found that the signal-to-noise ratio (SNR) was good for values of reflectivity > 25 dBZ at the 3-km level. In some scans, we found data that are not continuous (speckles), which are usually collected either in regions with low SNR where the dual-PRF scheme failed or in regions with strong turbulence where the unfolding scheme failed. Those speckles are removed using the standard deviation of Doppler velocity. Even with these corrections, there were still unrealistic Doppler velocities that were either not unfolded properly or erroneous. These values were excluded from VAD analysis.

The first step in performing VAD analysis is to collect measured Doppler velocity data V_r in a volume. The volume here refers to one complete 360° scan. This volume of data is divided into horizontal rings consisting of data at a specific elevation angle and range from the radar. Note that all angles discussed in this section and subsequent sections are in the track-relative coordinate system. Because of aircraft motion, elevation angles and ranges vary for each V_r in the ring. Since we use only the data with low roll and pitch angles (i.e., absence of turns and banks), such variation is small in general: ±2° for elevation and ±0.5 km in range. So we treat them as constant when using Eq. (2). Therefore in each ring, V_r is only a function of rotation angle θ. The second step is to check each ring of data for gaps in rotation angles. If the sum of all gaps is larger than 50°, the scan will not be processed. Scans with data missing beyond this threshold can create significant errors in the estimated velocity for each horizontal component.

b. Results from Tropical Storm Matthew

The VAD and dual-Doppler wind retrieval methods are first applied to HIWRAP observations of Tropical Storm Matthew collected on 24 September 2010. Braun et al. (2013) show a marked asymmetry of the precipitation with intense convection down shear produced by a northeasterly deep-layer (850–200 hPa) vertical wind shear of ~6 m s^{-1}. Figures 4a and 4c show the vertical cross section of reflectivity from the inner beam at Ku band between 0713 and 0738 UTC along the flight segment 9 shown in Figs. 13a,e in Braun et al.'s (2013) paper. We choose this segment because it contains a broad stratiform region. The melting band is at a height of about 4.8 km, and active convection is seen at a distance of around 100 km. The reflectivities observed by the fore and aft radar beams are quite similar. Therefore, the storm structure did not change very much over the time period it took for the fore and aft beams to scan the same regions. The aircraft flew at ~19-km altitude with an average speed of 176 m s^{-1}; the time difference between fore and aft views of the same region by the inner beam of the HIWRAP varies between 0.5 and 2 min from storm heights of 15 km to the surface. The slight difference of the melting-band height between the fore and aft looks of the radar beams is due to the aircraft being pitched up slightly so that the track-relative elevation angle varied with the azimuth angle. The differences at the beginning of the plot are due to the roll of the aircraft during a turn coming into the line. Figures 4b and 4d show the Doppler velocities from the fore and aft beams. The fore and aft Doppler velocities are different because the particle velocities are projected onto radials oriented 180° apart in rotation angle. Note that negative Doppler is toward the radar (upward) and positive is away from the radar (downward). In the following, we will first show the results from dual-Doppler analysis followed by the results from VAD analysis.

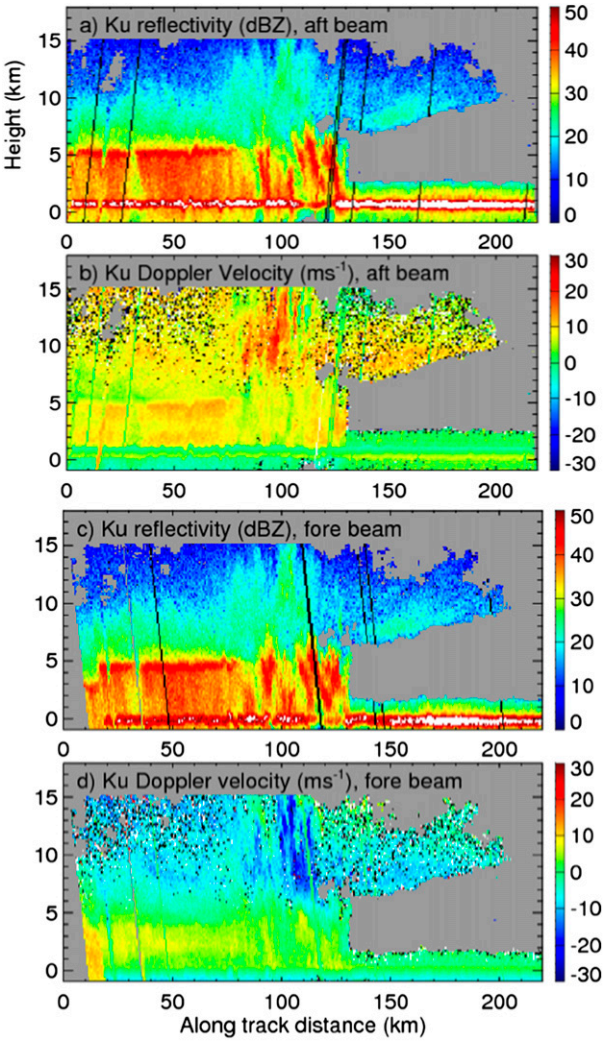

FIG. 4. Vertical cross section of HIWRAP observations of Tropical Storm Matthew from Ku-band inner beam during 0713–0738 UTC 24 Sep 2010. (a),(c) Reflectivity (dBZ) and (b),(d) Doppler velocity (m s^{-1}) from the aft beam and fore beams, respectively. Note that positive is away from the radar (downward) and negative is toward the radar (upward).

1) RESULTS FROM DUAL-DOPPLER ANALYSIS

We will consider only the wind retrieval in the nadir coplane in this paper. Our main purpose here is to check the consistency of the results between the two methods. The retrieval of 3D wind fields using the dual-Doppler analysis will be left for a future study. There were no corroborating data during the Global Hawk flights, except for rare occasions when the NASA DC-8 flew underneath. The dropsonde data are not available during Matthew for direct validation of VAD wind fields. The dual-Doppler analysis described in section 3b provides an independent retrieval to that from VAD analysis. An intercomparison between the two methods is not a direct validation, but it would help us to establish some confidence in the VAD-derived wind fields. Also, by combining the horizontal winds derived from VAD with W derived from the dual-Doppler analysis, divergence of horizontal wind fields can be estimated.

Figures 5a and 5b show vertical and horizontal components of the particle velocity in the nadir plane through the flight path. These were calculated using the dual-Doppler method applied to the nadir coplane [Eq. (16)]. Note that the vertical particle velocity shown in Fig. 5 is $W = w + V_t$. In the stratiform region, we see downward particle motions of about 5–10 m s^{-1} corresponding to rainfall speeds. Note also the sharp transition in the particle fall velocity through the melting band

as the snow particles melt into raindrops. In the convective region, the figure shows a strong updraft and downdraft extending from melting band to a height of about 12 km, at a distance of about 100 km. The shear of the horizontal wind in the nadir plane can be seen in the along-track component of the particle velocity. Note also that in the upper levels the computed winds are noisy because the dual-PRF unfolding scheme failed at the presence of low SNR or turbulence.

2) RESULTS FROM VAD ANALYSIS

Figures 5c and 5d show the results by performing VAD analysis for each scan circle along the flight track. Below about 7 km, the cross-track wind (Fig. 5c) is greater than 5 m s^{-1}. It is worth noting that the direction of the cross-track wind is defined as positive when the wind is pointing to the right of the flight track, or toward the southeast for this flight line. This is consistent with the streamlines at 700 hPa shown in Fig. 13a in Braun et al. (2013), which depicts the counterclockwise rotation of Tropical Storm Matthew. The along-track wind (Fig. 5d) agrees in general with that from the dual-Doppler analysis, even in the convective region.

For the comparison of VAD and dual-Doppler analysis, we selected a region with uniform stratiform rain indicated by the dashed triangle in Fig. 5a. Figure 6a shows the vertical profiles of the derived horizontal wind fields from VAD analysis. The vertical component of Doppler velocity ($W = w + V_t$) and along-track wind, calculated from dual-Doppler analysis, are averaged within the VAD volume. The along-track wind estimated from VAD analysis (dark blue dashed line in Fig. 6a) compares reasonably well with that from dual-Doppler analysis (dark blue solid line). Some discrepancy occurs near the melting layer. The cross-track wind (light blue line in Fig. 6a) is about 10 m s^{-1} below the melting layer and near zero at higher levels. Note the usual increase in the reflectivity through the melting band, which matches with a corresponding transition in the vertical particle velocity. Figure 6b shows DIV$_h$, the divergence of horizontal wind, calculated using Eq. (6). The divergence is practically zero from the lowest level of reliable data (2-km altitude) to about 1–2 km above the melting layer. From about 7- to 12-km height, the divergence decreases from 0 to about -4×10^{-3} s^{-1}. An in-depth analysis of Tropical Storm Matthew will be presented in future work.

c. *Results from Hurricane Karl*

To further test the performance of the VAD approach on HIWRAP data, we apply it to Hurricane Karl. During 16–17 September 2010, the Global Hawk overflew Karl during a period of rapid intensification with 20 crossings of the eye (Braun et al. 2013). HIWRAP collected Doppler radar data over a period of 14 h (1853–2346 UTC on 16 September to 0811 UTC on 17 September). Since this was HIWRAP's first science flight during GRIP, the performance of the HIWRAP's hardware and software, especially the sophisticated digital receiver subsystem, was still under improvement. The low SNR and noisy data resulted in large Doppler velocity folding errors, especially in the upper levels of the storm and near the eyewall. Table 2 lists 15 flight lines for Karl to obtain the horizontal wind fields.

Figure 7 shows the vertical cross section of one flight segment from southwest to northeast during 0331:47–0413:44 UTC. The reflectivity (Fig. 7a) shows a sloping

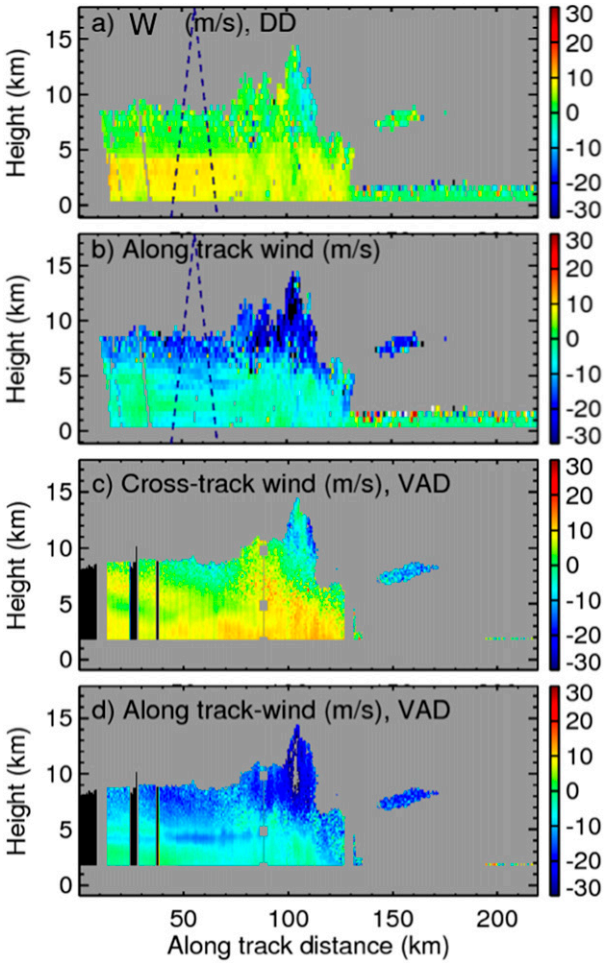

FIG. 5. (a) Hydrometeor vertical velocity W from the leg presented in Fig. 4. Positive values indicate downward motion. (b) Along-track wind calculated from fore and aft beams using dual-Doppler analysis; the triangle enclosed by the dashed lines shows the area covered by one scan for the inner beam. (c) Cross-track (positive is out of the page, from northwest to southeast) and (d) along-track wind components derived from VAD analysis (positive is from left to right, from southwest to northeast).

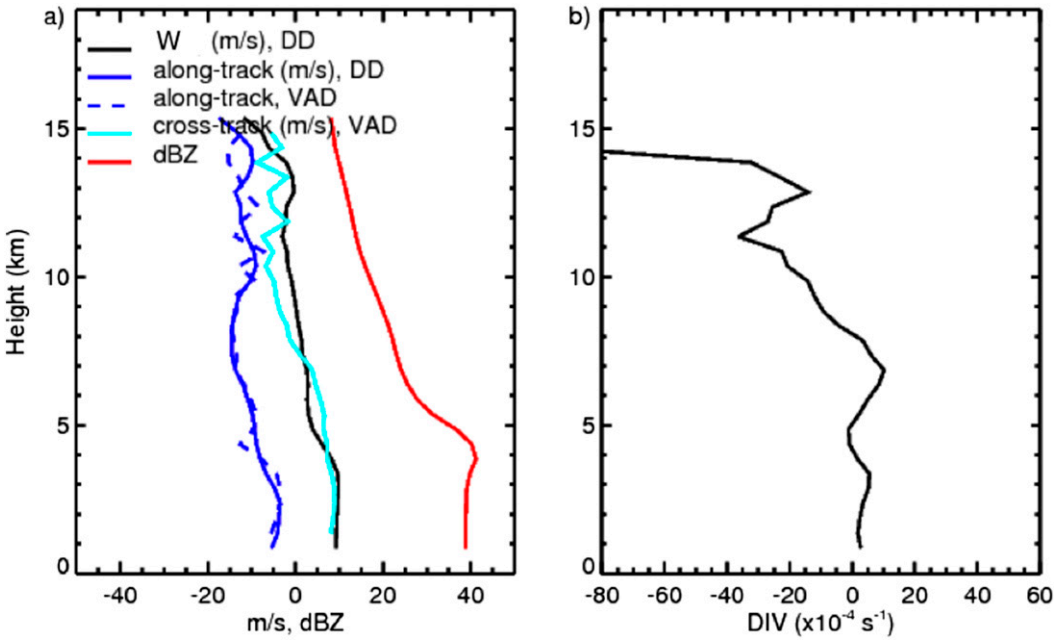

FIG. 6. (a) Vertical profiles of cross-track (cyan line) and along-track (dark blue dashed line) winds from VAD analysis at $Y = 53$ km from the leg in Fig. 4. For comparison, profiles of along-track wind from dual-Doppler analysis (dark solid blue line), hydrometeor vertical velocity W (black), and reflectivity (red) are averaged from all profiles within the triangle shown in Fig. 5a. (b) Divergence calculated from W and VAD fitting using Eq. (6).

eyewall and stratiform rain. Doppler velocity from the aft beam (Fig. 7b) shows mostly downward hydrometeor motion. The cross-track wind changed sign when aircraft crossed the hurricane eye located at around 150-km distance (Fig. 7c). Figure 8 shows the composite of VAD-derived winds from 10 flight lines at 3-km height. The flight lines have been adjusted to the Karl center at 0600 UTC given by NOAA National Hurricane Center (NHC) taking into account the movement of the storm center ($4\,\mathrm{m\,s^{-1}}$).

Dropsondes from the NASA DC-8 were used to validate the VAD-derived wind fields. Ten dropsondes were released from the DC-8 between 1911 and 2351 UTC on 16 September near the vicinity of HIWRAP flight lines between 1853 and 2346 UTC. No dropsondes from the DC-8 were available on 17 September. Figure 9 shows the locations of dropsonde relative to the flight line and wind fields from the drops and VAD analysis at 3-km height. As we can see, the VAD winds are in general agreement with the winds measured from sounding data. To examine the vertical variation of the wind, we locate one dropsonde that is nearly coincident with VAD-derived winds. The location of the drop is about 5 km from the location of the selected VAD profile. Figure 10 shows the comparison of the wind fields and directions between dropsonde and VAD-derived winds. The wind speed and direction from VAD analysis and those from the dropsonde are in general agreement at heights between 2 and 6 km. The poor agreement below 2 km is expected since the HIWRAP Doppler velocity estimate is affected by the pulse compression range sidelobes from the surface. Above 6 km, there is some discrepancy, which can be attributed to more noise existing in the measurements at these altitudes. Considering these factors and the difference in both time and space of the VAD and dropsonde measurements, the overall agreement between the two measurements is reasonably good.

5. Error due to variation of W and impact on tropical cyclone retrieval

The VAD technique presented in this paper relies on the assumption that the vertical hydrometeor velocity W is constant along each scan circle. Random errors in W due to signal fluctuation or turbulence do not affect the VAD-derived horizontal wind field. However, systematic changes of W either due to variation of vertical winds or the terminal velocity of particles along the scan circle introduce errors in horizontal wind estimates. Browning and Wexler (1968) showed that for ground-based radar, such error could be made acceptably small by scanning at appropriate elevations and range. For HIWRAP, elevation angles are set to $-60°$ and $-50°$ for

TABLE 2. The 16–17 September Karl flight lines.

	Time (UTC)	Flight orientation
01	1853:10–1919:18 16 Sep	N–S (sonde 2)
02	1938:29–1957:40 16 Sep	SW–NE
03	2009:56–2055:23 16 Sep	No good data
04	2109:24–2134:01 16 Sep	S–N
05	2319:49–2346:03 16 Sep	N–S (sonde 22)
1	0000:00–0024:30 17 Sep	SE–NW
2	003831–0117:02 17 Sep	SW–NE
3	0143:21–0223:41 17 Sep	N–S
4	0331:47–0413:44 17 Sep	SW–NE
5	0445:15–0525:39 17 Sep	N–S
6	0537:55–0600:45 17 Sep	SE–NW
7	0609:33–0650:11 17 Sep	Too many turns
8	0636:03–0650:11 17 Sep	N–S
9	0655:28–0709:33 17 Sep	SE–NW (short)
10	0759:38–0811:55 17 Sep	SE–NW (short)

the inner and outer beams, respectively. Such high elevation angles could result in larger errors in the parameters estimated from the VAD analysis. In this discussion, we will focus on errors in horizontal wind fields due to variation in W along the scan circle.

Assuming $W = W(\theta)$, a Fourier analysis for u velocity gives the following:

$$u_0' = u_0 + \frac{\sin\Phi}{\pi\cos\Phi}\int_0^{2\pi} W(\theta)\sin\theta\, d\theta = u_0 + \varepsilon_u, \qquad (18)$$

where $u_0' = u_0 = C_2/\cos\Phi$ if W is constant. The term in Eq. (18) defined as ε_u represents the error in u_0 due to W not being a constant along the scan circle. A similar expression can be derived for the error in v_0 (ε_v) as well as the errors for the other parameters. Unfortunately, we do not know W as a function of θ, but we do know W as a function of y along the nadir plane from the dual-Doppler analysis. For the purposes of estimating ε_u, we will assume that $W(y)$ in the nadir plane is equal to $W(\theta)$ for a given scan circle and altitude. Although this assumption may not be ideal, the nadir-plane W field captures realistic variations of W that are suitable for calculating realistic errors in the VAD-derived horizontal velocity.

For each scan circle, W values are taken from the nadir-plane dual-Doppler analysis over a length equivalent to the diameter of the scan circle, which varies from 6 to 18 km between altitudes of 14 and 3 km. These values of W are then distributed evenly along the scan circle. With these W values substituted into Eq. (18), it follows that the error at any point $y = j$ along the flight track is calculated by

$$\varepsilon_j \approx \frac{\sin\Phi}{\pi\cos\Phi}\sum_{i=j}^{j+\mathrm{nc}} W_i \sin\theta_i \Delta\theta_i, \quad j = 0, \ldots n, \qquad (19)$$

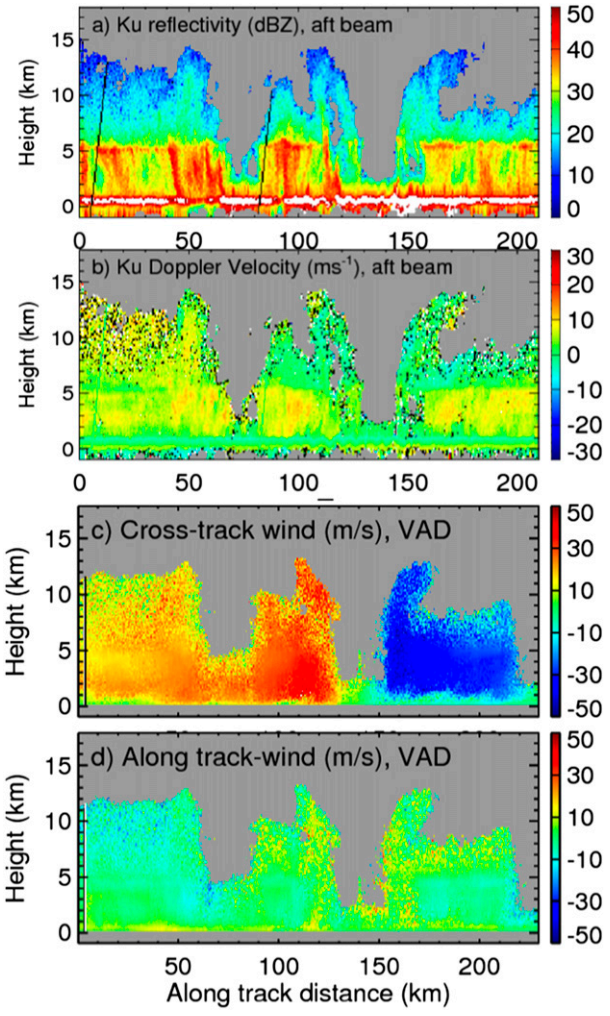

FIG. 7. Vertical cross section of HIWRAP observations of Hurricane Karl from 0331 to 0413 UTC 17 Sep 2010. (a) Reflectivity and (b) Doppler velocity for the Ku-band inner beam. Note that positive values indicate motion away from the radar (downward) and negative is toward the radar (upward). The clear region around 140-km distance is the eye of the hurricane. (c) Cross-track and (d) along-track wind fields from the VAD analysis.

where $\Delta\theta_i = 2\pi/nc$, $\theta_i = \Delta\theta_i \times \mathrm{nc}$, and nc is the number of W values taken from the dual-Doppler analysis within the specified length.

We examined the horizontal-velocity-error calculations using the data from Tropical Storm Matthew (Fig. 4) and Hurricane Karl (Fig. 7). Figure 11a shows the dual-Doppler W values along the nadir that were used in Eq. (19), and Fig. 11b shows the resulting errors in the cross-track wind u that were calculated from Eq. (19). The calculations are performed at two altitude levels. At the beginning of the flight leg, W values change very little. The higher-altitude W value remains

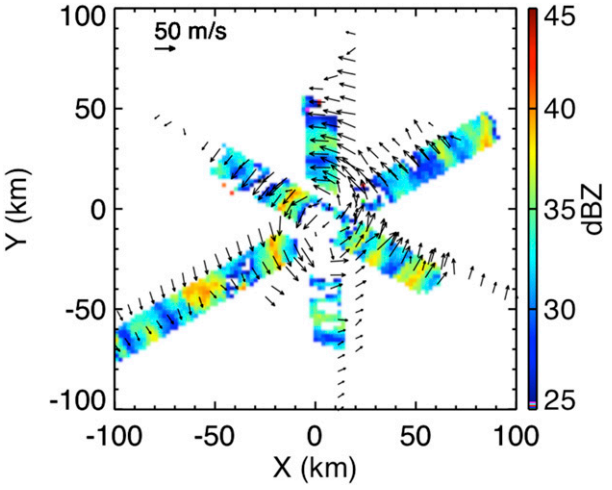

FIG. 8. Composite of VAD-derived wind fields at the 3-km level from 10 flight lines in Hurricane Karl (see Table 2) overlaid with reflectivity from the HIWRAP Ku band. For clarity, we show the reflectivity from only three flight lines.

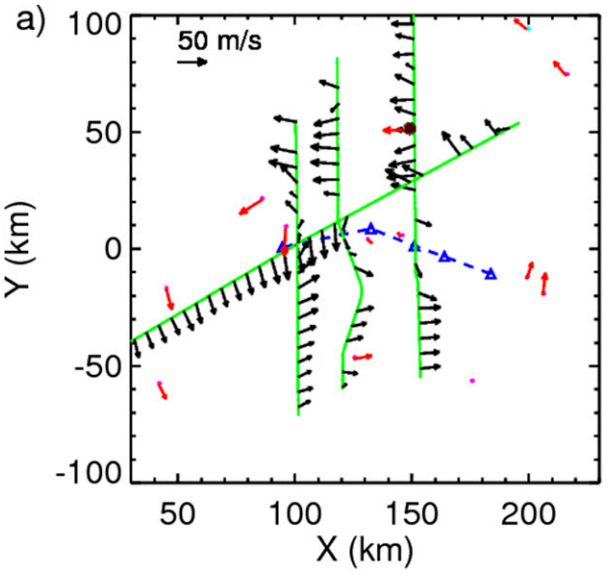

FIG. 9. Flight tracks (green) between 1853 and 2346 UTC 16 Sep from Hurricane Karl. The dashed blue line shows the center of the hurricane from NOAA P3 between 1711 and 2340 UTC. The wind vectors are from VAD analysis (black) and DC-8 dropsonde (red) at 3-km altitude. The large brown dot is the location of dropsonde released from the DC-8 around 1911:02 UTC. The winds from this sonde are used for comparison with VAD winds shown in Fig. 10.

near $3\,m\,s^{-1}$, while the lower-altitude W value remains near $9\,m\,s^{-1}$. Given the assumption of constant W, these relatively invariant values yield small errors, which are less than $1\,m\,s^{-1}$ in magnitude. These relatively invariant W values are also consistent with the stratiform precipitation that is displayed in the reflectivity signature (Fig. 4a). At 80-km distance, the W values begin to fluctuate between -4 and $14\,m\,s^{-1}$ for the upper level and between 3 and $14\,m\,s^{-1}$ for the lower level. Correspondingly, the error magnitudes increase, reaching $11\,m\,s^{-1}$. These findings demonstrate that areas of deep convection can produce significant errors in the VAD technique. As seen in Fig. 13 of Braun et al. (2013), the deep convection observed in Tropical Storm Matthew spanned over 35 km in distance along the center of the convective mass, which is larger than the diameter of the HIWRAP scan circle.

We also examined the error calculations from Hurricane Karl at 3.8-km altitude, which are shown in Fig. 12. The dual-Doppler analysis had noise near the weak reflectivity areas (e.g., $Y = 70$ km), so we applied a threshold to remove values of $W < -10\,m\,s^{-1}$, as these values were deemed to be unrealistic in this environment. The W values in Fig. 12a remained mostly in the range of 5–$10\,m\,s^{-1}$. The notable exceptions occurred at the eyewall passes at $Y = 125$ and $Y = 150$ km, where W values fluctuated within a range of $15\,m\,s^{-1}$. Figure 12b shows the estimated errors for both the cross-track (u) and along-track (v) winds. As expected, both ε_u and ε_v magnitudes remained less than $2\,m\,s^{-1}$ throughout the stratiform regions at $Y < 50$ km and $Y > 155$ km. The largest errors occur in the eyewall, with magnitudes reaching $19\,m\,s^{-1}$. These errors were not surprising since they coincided with the largest fluctuations in W. We have analyzed all of the Karl flight lines listed in Table 2 and found similar results.

The preceding results that estimate the error due to W variation further demonstrate how the VAD technique can be applied in the different regions of a tropical cyclone. In the stratiform regions of a tropical cyclone, the VAD technique captures the wind field with good accuracy. In stratiform regions, the horizontal wind field varies slowly over distance, which allows for the assumption of linear wind fields to hold well and produce small errors; furthermore, the errors from the circle approximation and the assumption of a constant W combine to produce errors less than $3\,m\,s^{-1}$ for each wind component.

Regions of deep convection, particularly with length scales equal to or larger than the HIWRAP scan circle, present the largest challenge to the VAD technique's ability to provide mean wind fields. Such regions include the tropical cyclone eyewall. Errors can accrue in the eyewall region since the linear approximation may not hold well, and as seen in section 3, errors due to the closed-circle approximation are elevated. Additionally, errors near $10\,m\,s^{-1}$ can occur when hydrometeor vertical velocities shift by $20\,m\,s^{-1}$ within a scan circle, which is possible in the eyewall region.

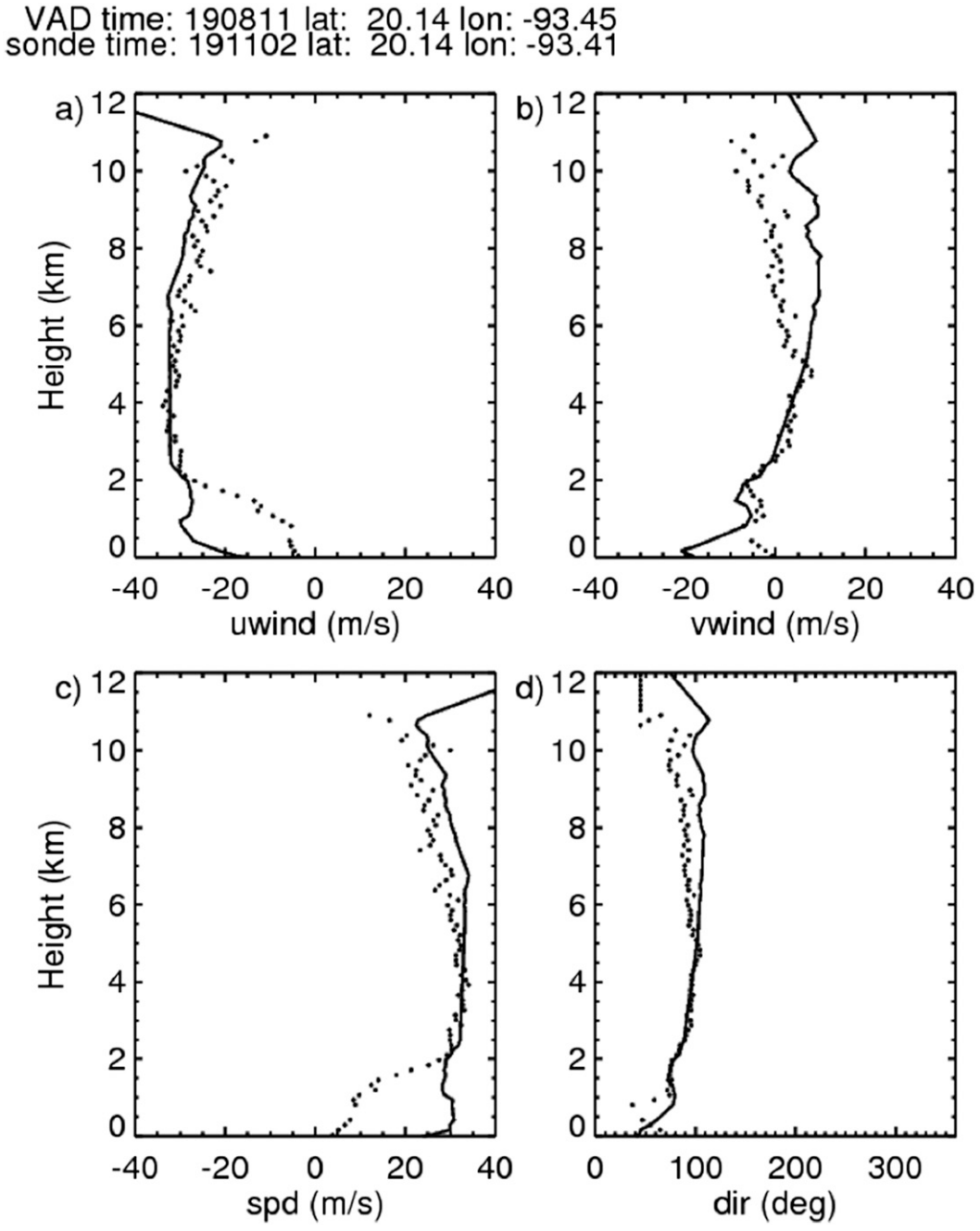

FIG. 10. Vertical profiles of (a) east wind (uwind), (b) north wind (vwind), (c) wind speed (spd), and (d) direction (dir) from the dropsonde (solid line) and VAD analysis (dotted line) indicated in Fig. 9.

Despite these possible errors, the VAD-derived cross-track wind in Fig. 7c depicts the expected wind pattern of a tropical cyclone eyewall, showing a cyclonic circulation with elevated winds toward the storm center. The VAD analysis can thus capture the large-scale vortex structure, but the user must keep in mind that exact values in wind speed in the eyewall can contain errors on the same order of magnitude as the wind speed. Active convection that is not deep and on the same scale as the scan circle may still yield accurate VAD-derived winds. Shallow convection has vertical velocities that span a smaller range and thus yield lower errors due to the assumption of constant W. Also, deep convection that is smaller in scale than the scan circle is less likely to be

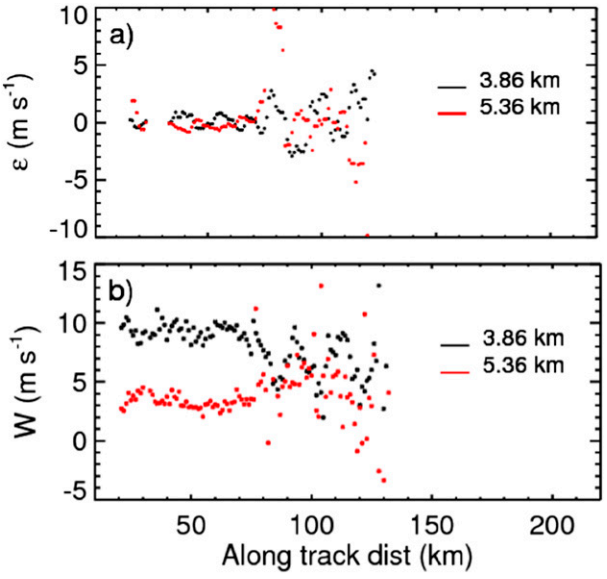

FIG. 11. (a) Estimated errors ε in cross-track wind u due to W not being a constant along the circle at heights of 3.86 and 5.36 km for the Matthew flight line shown in Fig. 5. (b) The W values along the flight line at the same two heights.

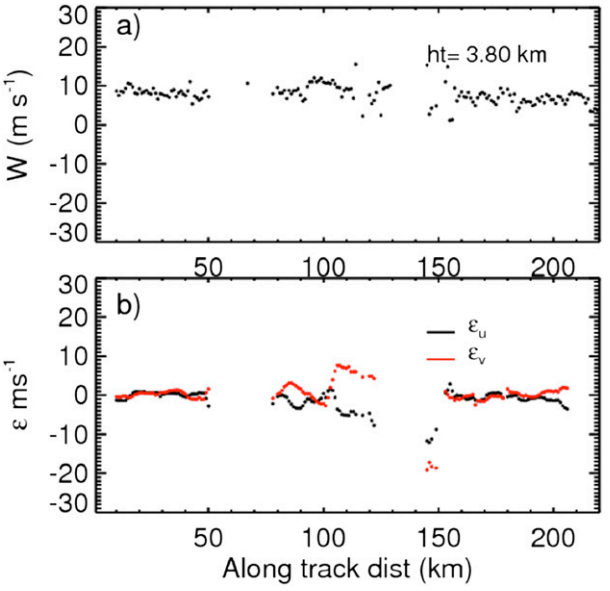

FIG. 12. (a) The W and (b) the estimated errors ε in cross-track wind due to W not being a constant along the circle at a height of 3.86 for the Karl flight line shown in Fig. 7.

captured in the VAD analysis, as other data within the scan circle can drive the calculation of the mean larger-scale horizontal wind.

6. Conclusions

In this paper, the VAD analysis technique established for ground-based radar is successfully applied to the data obtained from the airborne, downward, conically scanning HIWRAP radar. The VAD technique provides a mean vertical profile of the horizontal winds, which is obtained from synthesizing data over each complete conical scan of the HIWRAP radar. The VAD technique is computationally inexpensive, which makes it suitable for real-time retrievals of the mean wind field. These retrievals can be used for making real-time flight decisions, improving forecasts of storm evolution, and providing the vertical structure for general context in case studies.

The VAD technique is compared with a dual-Doppler analysis technique that is based on the coplane method developed for ground-based radar. The main difference between the ground-based and the airborne radar is the orientation of the so-called zero coplane. For ground-based radar, the zero coplane is the surface where the boundary condition can be specified easily. But for HIWRAP scanning geometry, the zero coplane is the vertical plane under the flight track, and the boundary condition is unknown. A method to solve this problem, and to subsequently retrieve three-dimensional winds from HIWRAP observations, is presented by Didlake et al. (2015). In this paper, we mainly focused on dual-Doppler analysis at nadir. For the vertical plane under the flight track, we found that errors in the horizontal wind speed along the flight track and vertical hydrometeor velocity are less than $2\,\mathrm{m\,s^{-1}}$ because of signal fluctuation.

We have applied the VAD analysis to the first HIWRAP field data collected during the NASA GRIP mission. Two cases are presented: the first is a stratiform case from Tropical Storm Matthew and the second is from Hurricane Karl. For the Matthew case, we first calculated the along-track wind and hydrometeor fall speed using the dual-Doppler analysis and then used the VAD method to derive the horizontal wind fields. The results show that the along-track wind from VAD and dual-Doppler analysis in the nadir plane agree in general. To calculate the divergence using VAD analysis, we have used vertical velocity derived from the dual-Doppler synthesis. For the Karl case, we retrieved horizontal winds from 15 h of flight data collected by HIWRAP. The results capture the mean vortex structure of Karl and provide valuable information for data assimilation. A comparison of the VAD-derived horizontal wind fields with that from a nearby dropsonde shows good agreement between 2- and 6-km altitudes.

We also examined the errors in the estimated VAD winds that arise because of the assumptions made for the

VAD calculations. One assumption is that a complete conical scan of the HIWRAP beam maps out a perfect circle rather than the actual spiral that is outlined as a result of the moving aircraft platform. For typical values of HIWRAP scan rate and aircraft ground speed, the horizontal wind speed errors due to this assumption are less than $0.5\,m\,s^{-1}$ in stratiform regions where the horizontal wind gradient is less than $10^{-3}\,s^{-1}$. Another assumption is that the vertical hydrometeor velocity remains constant along a complete conical scan. Using the dual-Doppler analysis from Matthew and Karl, we found that this assumption can produce errors near $10\,m\,s^{-1}$ in regions of deep convection such as the eyewall; while in stratiform regions, this assumption produces errors less than $2\,m\,s^{-1}$.

The VAD winds represent a mean over an area within the radar scan region and therefore smooth out many of the transient or small-scale features so that only the larger mesoscale and synoptic-scale features of the winds remain. For hurricanes, the wind fields within a HIWRAP scan circle do not exactly align with the necessary assumptions for the VAD technique. As a result, the VAD method may not capture detailed structures, but it still can capture large-scale features, such as the mean vortex structure, when combining the VAD analysis from multiple flight legs. Such information has tremendous value for data assimilation and for operational forecasts of storm location and intensity. The VAD technique can also be used to examine other precipitating systems like midlatitude cyclones.

Although the HIWRAP dataset from GRIP presented many challenges, the VAD technique successfully used this dataset to discern the mean vortex structures. Since GRIP, HIWRAP has flown in multiple field campaigns and collected precipitation and wind observations with significantly improved data quality. Future work will include applying the VAD technique to the improved datasets and developing a real-time VAD system for upcoming field experiments.

Acknowledgments. We thank Professor Ramesh Srivastava for insightful discussions and for suggesting some of the analysis method. We also thank Dr. Jason Sippel for stimulating discussions on using Doppler radar data for data assimilation and Matthew McLinden, Jaime Cervantes, Martin Perrine, and Ed Zenker for engineering support and HIWRAP data processing. Funding for this work came from the NASA Hurricane Science Research Program under Dr. Ramesh Kakar and the Hurricane and Severe Storm Sentinel investigation under NASA's Earth Venture Program.

REFERENCES

Armijo, L., 1969: A theory for the determination of wind and precipitation velocities with Doppler radars. *J. Atmos. Sci.,* **26,** 570–573, doi:10.1175/1520-0469(1969)026<0570:ATFTDO>2.0.CO;2.

Braun, S., and Coauthors, 2013: NASA's Genesis and Rapid Intensification Processes (GRIP) field experiment. *Bull. Amer. Meteor. Soc.,* **94,** 345–363, doi:10.1175/BAMS-D-11-00232.1.

Browning, K. A., and R. Wexler, 1968: The determination of kinematic properties of a wind field using Doppler radar. *J. Appl. Meteor.,* **7,** 105–113, doi:10.1175/1520-0450(1968)007<0105:TDOKPO>2.0.CO;2.

Chong, M., and J. Testud, 1996: Three-dimensional air circulation in a squall line from airborne dual-beam Doppler radar data: A test of coplane methodology software. *J. Atmos. Oceanic Technol.,* **13,** 36–53, doi:10.1175/1520-0426(1996)013<0036:TDACIA>2.0.CO;2.

Dazhang, T., S. G. Geotis, R. E. Passarelli Jr., A. L. Hansen, and C. I. Frush, 1984: Evaluation of an alternating-PRF method for extending the range of unambiguous Doppler velocity. Preprints, *22nd Conf. on Radar Meteorology,* Zurich, Switzerland, Amer. Meteor. Soc., 523–527.

Didlake, A. C., Jr., and R. A. Houze Jr., 2009: Convective-scale downdrafts in the principal rainband of Hurricane Katrina (2005). *Mon. Wea. Rev.,* **137,** 3269–3293, doi:10.1175/2009MWR2827.1.

——, and ——, 2013: Dynamics of the stratiform sector of a tropical cyclone rainband. *J. Atmos. Sci.,* **70,** 1891–1911, doi:10.1175/JAS-D-12-0245.1.

——, G. M. Heymsfield, L. Tian, and S. R. Guimond, 2015: The coplane analysis technique for three-dimensional wind retrieval using the HIWRAP airborne Doppler radar. *J. Appl. Meteor.,* **54,** 605–623, doi:10.1175/JAMC-D-14-0203.1.

Gamache, J. F., 1997: Evaluation of a fully three-dimensional variational Doppler analysis technique. Preprints, *28th Conf. on Radar Meteorology,* Austin, TX, Amer. Meteor. Soc., 422–423.

Gao, J., M. Xue, A. Shapiro, and K. K. Droegemeier, 1999: A variational method for the analysis of three-dimensional wind fields from two Doppler radars. *Mon. Wea. Rev.,* **127,** 2128–2142, doi:10.1175/1520-0493(1999)127<2128:AVMFTA>2.0.CO;2.

——, K. K. Droegemeier, J. Gong, and Q. Xu, 2004: A method for retrieving mean horizontal wind profiles from single-Doppler radar observations contaminated by aliasing. *Mon. Wea. Rev.,* **132,** 1399–1409, doi:10.1175/1520-0493-132.1.1399.

Guimond, S. R., L. Tian, G. M. Heymsfield, and S. J. Frasier, 2014: Wind retrieval algorithms for the IWRAP and HIWRAP airborne Doppler radars with applications to hurricanes. *J. Atmos. Oceanic Technol.,* **31,** 1189–1215, doi:10.1175/JTECH-D-13-00140.1.

Heymsfield, G. M., and Coauthors, 1996: The EDOP radar system on the high-altitude NASA ER-2 aircraft. *J. Atmos. Oceanic Technol.,* **13,** 795–809, doi:10.1175/1520-0426(1996)013<0795:TERSOT>2.0.CO;2.

——, L. Tian, L. Li, M. McLinden, and J. I. Cervantes, 2013: Airborne radar observations of severe hailstorms: Implications for future spaceborne radar. *J. Appl. Meteor. Climatol.,* **52,** 1851–1867, doi:10.1175/JAMC-D-12-0144.1.

Hildebrand, P. H., and Coauthors, 1996: The ELDORA/ASTRAIA airborne Doppler weather radar: High-resolution observations from TOGA COARE. *Bull. Amer. Meteor.*

Soc., **77,** 213–232, doi:10.1175/1520-0477(1996)077<0213:TEADWR>2.0.CO;2.

Jorgensen, D. P., P. H. Hildebrand, and C. L. Frush, 1983: Feasibility test of an airborne pulse-Doppler meteorology radar. *J. Climate Appl. Meteor.,* **22,** 744–757, doi:10.1175/1520-0450(1983)022<0744:FTOAAP>2.0.CO;2.

——, T. Matejka, and J. D. DuGranrut, 1996: Multi-beam techniques for deriving wind fields from airborne Doppler radars. *Meteor. Atmos. Phys.,* **59,** 83–104, doi:10.1007/BF01032002.

Lee, W.-C., P. Dodge, F. D. Marks, and P. H. Hildebrand, 1994: Mapping of airborne Doppler radar data. *J. Atmos. Oceanic Technol.,* **11,** 572–578, doi:10.1175/1520-0426(1994)011<0572:MOADRD>2.0.CO;2.

Lhermitte, R. M., and D. Atlas, 1961: Precipitation motion by pulse Doppler radar. *Proc. Ninth Weather Radar Conf.,* Kansas City, MO, Amer. Meteor. Soc., 218–223.

Li, L., G. M. Heymsfield, J. Carswell, D. Schaubert, J. Creticos, and M. Vega, 2008: High-Altitude Imaging Wind and Rain Airborne Radar (HIWRAP). *Proc. IEEE Int. Geoscience and Remote Sensing Symp. (IGARSS) 2008,* Boston, MA, IEEE, 354–357.

Marks, F. D., and R. A. Houze, 1987: Inner core structure of Hurricane Alicia from airborne Doppler radar observations. *J. Atmos. Sci.,* **44,** 1296–1317, doi:10.1175/1520-0469(1987)044<1296:ICSOHA>2.0.CO;2.

Matejka, T., and R. C. Srivastava, 1991: An improved version of the extended velocity-azimuth display analysis of single-Doppler radar data. *J. Atmos. Oceanic Technol.,* **8,** 453–466, doi:10.1175/1520-0426(1991)008<0453:AIVOTE>2.0.CO;2.

Michelson, S. A., and N. L. Seaman, 2000: Assimilation of NEXRAD-VAD winds in summertime meteorological simulations over the northeastern United States. *J. Appl. Meteor.,* **39,** 367–383, doi:10.1175/1520-0450(2000)039<0367:AONVWI>2.0.CO;2.

Miller, L. J., and R. G. Strauch, 1974: A dual Doppler radar method for the determination of wind velocities within precipitating weather systems. *Remote Sens. Environ.,* **3,** 219–235, doi:10.1016/0034-4257(74)90044-3.

Mohr, C. G., L. J. Miller, R. L. Vaughan, and H. W. Frank, 1986: The merger of mesoscale datasets into a common Cartesian format for efficient and systematic analyses. *J. Atmos. Oceanic Technol.,* **3,** 143–161, doi:10.1175/1520-0426(1986)003<0143:TMOMDI>2.0.CO;2.

Ray, P. S., D. P. Jorgensen, and S.-L. Wang, 1985: Airborne Doppler radar observations of a convective storm. *J. Climate Appl. Meteor.,* **24,** 687–698, doi:10.1175/1520-0450(1985)024<0687:ADROOA>2.0.CO;2.

Sippel, J. A., S. A. Braun, F. Zhang, and Y. Weng, 2013: Ensemble Kalman filter assimilation of simulated HIWRAP Doppler velocity data in a hurricane. *Mon. Wea. Rev.,* **141,** 2683–2704, doi:10.1175/MWR-D-12-00157.1.

——, F. Zhang, Y. Weng, L. Tian, G. M. Heymsfield, and S. A. Braun, 2014: Ensemble Kalman filter assimilation of HIWRAP observations of Hurricane Karl (2010) from the unmanned Global Hawk aircraft. *Mon. Wea. Rev.,* **142,** 4559–4580, doi:10.1175/MWR-D-14-00042.1.

Srivastava, R. C., T. J. Matejka, and T. J. Lorello, 1986: Doppler radar study of the trailing anvil region associated with a squall line. *J. Atmos. Sci.,* **43,** 356–377, doi:10.1175/1520-0469(1986)043<0356:DRSOTT>2.0.CO;2.

Sun, J., and Y. Zhang, 2008: Analysis and prediction of a squall line observed during IHOP using multiple WSR-88D observations. *Mon. Wea. Rev.,* **136,** 2364–2388, doi:10.1175/2007MWR2205.1.

Testud, J., P. H. Hildebrand, and W.-C. Lee, 1995: A procedure to correct airborne Doppler radar data for navigation errors using the echo returned from the earth's surface. *J. Atmos. Oceanic Technol.,* **12,** 800–820, doi:10.1175/1520-0426(1995)012<0800:APTCAD>2.0.CO;2.